ACS APPLIED POLYMER MATERIALS

Article

Cite This: ACS Appl. Polym. Mater. 2019, 1, 3039−3047

pubs.acs.org/acsapm

# Luminescent Solar Concentrators Based on Energy Transfer from an Aggregation-Induced Emitter Conjugated Polymer

Guanpeng Lyu,[†] James Kendall,[†] Ilaria Meazzini,[†] Eduard Preis,[‡] Sebnem Bayseç,[‡] Ullrich Scherf,[‡] Sébastien Clément,[§] and Rachel C. Evans*[,†]

[†]Department of Materials Science and Metallurgy, University of Cambridge, 27 Charles Babbage Road, Cambridge CB3 0FS, United Kingdom

[‡]Macromolecular Chemistry Group (buwmakro) and Institute for Polymer Technology, Bergische Universität Wuppertal, Gausss-Strasse 20, D-42119 Wuppertal, Germany

[§]Institut Charles Gerhardt Montpellier, ICGM, UMR 5253, CNRS, Université de Montpellier, ENSCM, Place Eugène Bataillon, 34095 Montpellier Cedex 5, France

Supporting Information

**ABSTRACT:** Luminescent solar concentrators (LSCs) are solar-harvesting devices fabricated from a transparent waveguide that is doped or coated with lumophores. Despite their potential for architectural integration, the optical efficiency of LSCs is often limited by incomplete harvesting of solar radiation and aggregation-caused quenching (ACQ) of lumophores in the solid state. Here, we demonstrate a multilumophore LSC design that circumvents these challenges through a combination of nonradiative Förster resonance energy transfer (FRET) and aggregation-induced emission (AIE). The LSC incorporates a green-emitting poly(tetraphenylethylene), p-O-TPE, as an energy donor and a red-emitting perylene bisimide molecular dye (PDI-Sil) as the energy acceptor, within an organic−inorganic hybrid diureasil waveguide. Steady-state photoluminescence studies demonstrate the diureasil host induced AIE from the p-O-PTE donor polymer, leading to a high photoluminescence quantum yield (PLQY) of ∼45% and a large Stokes shift of ∼150 nm. Covalent grafting of the PDI-Sil acceptor to the siliceous domains of the diureasil waveguide also inhibits nonradiative losses by preventing molecular aggregation. Due to the excellent spectral overlap, FRET was shown to occur from p-O-TPE to PDI-Sil, which increased with acceptor concentration. As a result, the final LSC (4.5 cm × 4.5 cm × 0.3 cm) with an optimized donor−acceptor ratio (1:1 by wt %) exhibited an internal photon efficiency of 20%, demonstrating a viable design for LSCs utilizing an AIE-based FRET approach to improve the solar-harvesting performance.

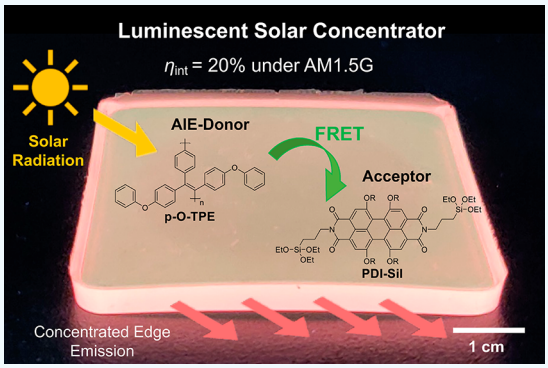


**KEYWORDS:** *aggregation-induced emission, conjugated polymer, energy transfer, organic−inorganic hybrid, luminescent solar concentrator*

## 1. INTRODUCTION

Luminescent solar concentrators (LSCs) are solar-harvesting devices fabricated from a transparent waveguide that is doped or coated with a luminescent species (lumophores).[1] LSCs collect solar radiation over a large surface area, upon which it is spectrally converted via a photoluminescence (PL) process and redirected to the edges of the device where photovoltaic (PV) cells can be mounted.[1,2] LSCs collect and concentrate both diffuse and direct sunlight, making them particularly desirable for use in regions with high building density or excessive cloud coverage.[3] These factors, combined with their aesthetic appeal and the diverse range of geometries that can be designed, mean that LSCs offer an excellent complementary approach for the architectural integration of PV technology in cities.[4]

LSCs were first proposed in the mid-1970s[5] and initially focused on rare-earth-doped glasses.[6,7] LSCs fabricated from organic materials have also become increasingly popular.[8−10] The combination of waveguide and lumophore used in an LSC is critical to its optical efficiency.[11] The ideal waveguide will have high transmittance across the solar spectrum and a refractive index, $n$, of around 1.5−2.0 to minimize reflective losses at the top surface, while maximizing the trapping efficiency of the radiation emitted within the waveguide.[11] The lumophore must have a photoluminescence quantum yield (PLQY) close to 100%, a high absorption coefficient and broad spectral overlap with the solar spectrum, and a large Stokes shift to minimize reabsorption losses.[3,11] Both the waveguide

Received: August 1, 2019
Accepted: September 19, 2019
Published: October 18, 2019




DOI: 10.1021/acsapm.9b00718
ACS Appl. Polym. Mater. 2019, 1, 3039−3047

and lumophore should have good photo- and thermal stability and easy processability for large-scale production.[10]

In recent decades, lumophores with high PLQYs and excellent stabilities, such as quantum dots (QDs),[12,13] metal complexes,[14,15] and organic dyes,[8−10,16,17] have been developed. In particular, $\pi$-conjugated polymers have been extensively investigated as lumophores for flexible, lightweight optical devices such as field-effect transistors,[18,19] organic light-emitting diodes,[20−22] and PV devices,[23,24] as well as LSCs,[25−27] due to their desirable optoelectronic properties and cost-effective solution processability. However, the optical efficiency of conjugated polymers is often undermined by aggregation-caused quenching (ACQ), which occurs due to preferential nonradiative relaxation of excited states as a result of intermolecular $\pi-\pi$ interactions.[11,28,29] This is especially problematic at high lumophore concentrations in solid host matrixes and can be detrimental to the optical efficiencies of LSCs.[17,30,31] The effect of ACQ can be mitigated by using lumophores that exhibit aggregation-induced emission (AIE).[29−33] For AIE-active molecules (i.e., AIEgens), nonradiative deactivation is significantly reduced in the aggregated state due to physical restraints on both intramolecular rotations and $\pi-\pi$ stacking due to the highly twisted molecular core.[33] This leads to preferential radiative relaxation of the excited state upon aggregation, i.e., the PL is "switched on".

The first reported AIE-based LSC incorporated tetraphenylethylene (TPE) in a poly(methyl methacrylate) (PMMA) film cast on a glass substrate.[30] This device was able to effectively concentrate light without inducing ACQ, even at an elevated lumophore concentration of 10 wt %. However, the emission range of TPE ($\lambda_{em} \approx 450$ nm) was not well-matched with the typical band gaps of silicon or GaAs solar cells.[30] This issue was later circumvented through Förster resonance energy transfer (FRET) from a molecular AIEgen donor (D) to an acceptor (A) lumophore co-doped in the waveguide, leading to an effective red shift in the emission.[17,31] An alternative approach to further tune the AIEgen emission to lower energy is to extend the $\pi$-conjugation of the molecule using electron donor and acceptor moieties.[34] For example, the TPE analogue, TPE-AC, which contains dimethylamine and malononitrile substituents appended to the core, was shown to exhibit intense red emission in both PMMA and polycarbonate matrixes; however, fluorescence quenching was still observed at concentrations above 0.6−0.7 wt % due to the formation of less emissive supramolecular-amorphous aggregates.[34] Recently, a tandem-structure LSC consisting of layers of N-doped carbon dots and red-emitting AIEgens was also reported.[35]

While the potential of both small-molecule AIEgens and conjugated polymers as lumophores for LSCs has been demonstrated, LSCs based on conjugated polymers with AIE characteristics have not yet been reported. A conjugated polymer analogue of TPE, poly(diphenoxy-tetraphenylethylene) (p-O-TPE) has a high PLQY (52−73%) and large Stokes shift (~150 nm) in the solid state,[36,37] suggesting that it could be successfully implemented in LSCs. However, as p-O-TPE is a green emitter, it would be advantageous to design a FRET-based LSC that additionally incorporates a red-emitting acceptor lumophore to increase the overlap with the spectral response (i.e., the external quantum efficiency spectrum) of standard Si PV cells. As a $\pi$-conjugated polymer, p-O-TPE has the additional advantage of accommodating fast exciton migration along its backbone.[25] This can be easily intercepted by a small amount of energy acceptors present in the matrix, thus making the FRET process efficient. The choice of waveguide is also important because both the donor and acceptor lumophores must be well-dispersed through the host. A family of organic−inorganic hybrid polymers known as ureasils have been demonstrated as excellent waveguides for LSCs[27,38−40] and other optical applications.[41] As hybrid materials, ureasils combine the easy processability and chemical functionality of organic polymers with the high optical transparency and stability of the typical inorganic waveguides.[11] Moreover, they can be easily fabricated into various shapes through a sol−gel process, making them compatible with a variety of architectural designs.[42,43]

Here, we investigate the design, PL properties, and optical efficiency of FRET-based LSCs incorporating p-O-TPE as the donor and perylene carboxdiimide-bridged triethoxysilane (PDI-Sil) as the acceptor, embedded within a diureasil waveguide. We postulated that the structure of the ureasil, in particular, the apolar nature of the alkyl-shielded siloxane backbone,[44] may help to induce the aggregation of p-O-TPE, thus enhancing the emission efficiency in the solid state. PDI-Sil is a red emitter related to the archetypal LSC lumophore Lumogen Red 305 (LR305). While LR305 shows a tendency to aggregate in ureasils,[10] we have recently shown that by covalently grafting the PDI-Sil analogue to the siloxane backbone of the ureasil aggregation can be effectively reduced, leading to high PLQYs (~80%).[39] Herein, we show that, due to excellent spectral overlap, p-O-TPE and PDI-Sil act as an efficient FRET pair in a ureasil waveguide. We observe that FRET also leads to reduced nonradiative relaxation of the p-O-TPE donor and extends the solar-harvesting window of the final LSC, giving rise to improved optical quantum efficiencies.

## 2. EXPERIMENTAL SECTION

**Materials.** Bis(2-aminopropyl) polypropylene glycol-*block*-polyethylene glycol-*block*-polypropylene glycol (Jeffamine ED-600, $M_w$ = 600 g mol$^{-1}$) and 3-(triethoxysilyl)propylisocyanate (ICPTES, 95.0%) were purchased from Sigma-Aldrich. Tetrahydrofuran (THF, ≥99.9%), ethanol (EtOH, 95.0%), and hydrochloric acid (HCl, 37%) were purchased from Fisher Scientific. Water was obtained from a Millipore Simpak 2 water purification system. p-O-TPE[36] ($M_n$ = 18,600 g mol$^{-1}$, $M_W$ = 36,700 g mol$^{-1}$) and *N*,*N*-bis(3-triethoxysilylpropyl)-1,6,7,12-tetra-*tert*-butylphenoxyperylene-3,4:9,10-tetra-carboxdiimide[39] were synthesized as previously reported. All materials were used as received.

**Fabrication of Diureasil-Based LSCs.** Samples containing p-O-TPE doped in diureasils (denoted p-O-TPE-dU(600)) at different concentrations (wt %) were prepared via a two-step sol−gel process. In the first step, ICPTES (0.91 mL, 3.68 mmol) was mixed with Jeffamine ED-600 (1.00 mL, 1.75 mmol) in THF (5 mL). The reaction mixture was refluxed at 70 °C for 24 h to obtain "one batch" of the organic−inorganic hybrid precursor, diureapropyltriethoxysilane (d-UPTES) in solution. The requisite volume, based on the final dopant concentrations of 0.001, 0.005, 0.01, and 0.05 wt % (with respect to the mass of the dry monoliths, "one batch" of d-UPTES yields a dry monolith of 1.76 g), of a stock solution of p-O-TPE (1 mg mL$^{-1}$ in THF) was the added to the d-UPTES solution under stirring. In the second step, gelling reagents (ethanol, HCl (0.5 M) and water) were added to the d-UPTES in sequence and thoroughly mixed. The molar ratio of Jeffamine ED-600:ethanol:HCl: water used was 88:345:1:265. The resulting mixture was poured into a polypropylene mold and gelled into free-standing monoliths. The mold was sealed with Parafilm M to allow slow evaporation of the excess THF in the samples over 5 days, followed by further oven drying at 40 °C for 3 days. "One batch" or "four batches" of the d-UPTES can be used to


DOI: 10.1021/acsapm.9b00718
ACS Appl. Polym. Mater. 2019, 1, 3039−3047

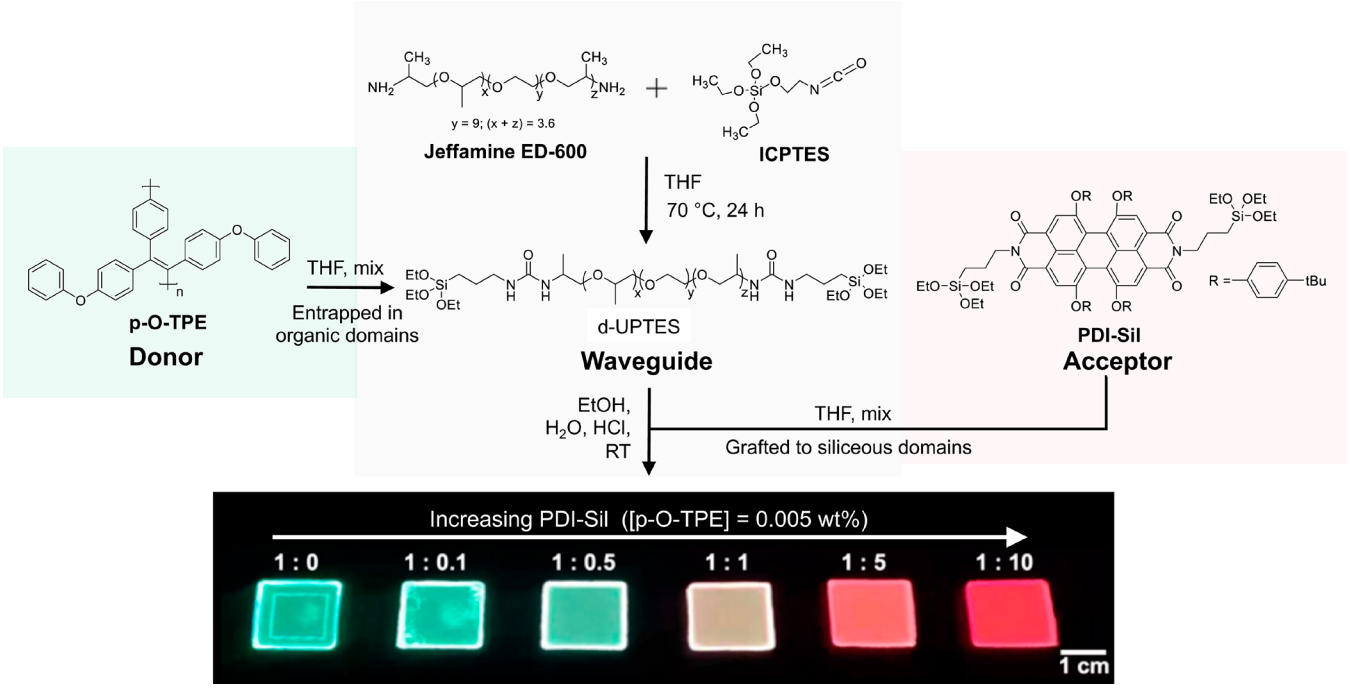


**Figure 1.** Synthetic route for the preparation of donor−acceptor LSCs. The conjugated polymer donor p-O-TPE is entrapped within the organic domains of the diureasil waveguide, while molecular acceptor PDI-Sil is covalently grafted to the siliceous network as a result of the hydrolysis and co-condensation between the triethoxysilyl groups of PDI-Sil and d-UPTES under the acidic conditions of the sol−gel process. The donor−acceptor ratio is varied to tune to emission of the final LSCs, as illustrated by the photograph of the final samples under UV light (365 nm). We note that when observed with the naked eye, the PL of these samples is generally homogeneous. The concentration of p-O-TPE is fixed at 0.005 wt % for p-O-TPE-PDI-Sil-dU(600) (top row), while the concentration of PDI-Sil is increased from 0 to 0.075 wt %. The ratios correspond to the p-O-TPE to PDI-Sil proportions.

fabricate "small" (2 cm × 2 cm × 0.3 cm) or "large" (4.5 cm × 4.5 cm × 0.3 cm) monoliths, respectively.

A similar approach was employed for the synthesis of PDI-Sil-dU(600), where the requisite volume of a stock solution of PDI-Sil in THF (1 mg $mL^{-1}$) was premixed with the d-UPTES solution under stirring prior to the addition of gelling reagents to obtain PDI-Sil concentrations of 0.0005, 0.0025, 0.005, 0.01, and 0.05 wt % with respect to the mass of the dry monolith. The addition of the gelling reagents triggers the hydrolysis and co-condensation between the triethoxysilyl groups of PDI-Sil and d-UPTES, leading to covalent grafting of PDI-Sil to the dU(600) framework.[39]

To obtain p-O-TPE-PDI-Sil-dU(600), a fixed volume of the stock solution of p-O-TPE (1 mg $mL^{-1}$ in THF) was first added to the d-UPTES solution to obtain a fixed concentration of 0.005 wt % in the final samples. This was followed by the addition of the PDI-Sil stock solution (1 mg $mL^{-1}$ in THF) with volume adjusted to obtain the desired p-O-TPE:PDI-Sil concentration ratios (by wt %) of 1:0, 1:0.1, 1:0.5, 1:1, 1:5, and 1:10 in the final samples.[39]

**UV/Vis Absorption Spectroscopy.** UV/vis absorption and transmittance spectra were measured with a PerkinElmer Lambda 750 spectrophotometer using wavelength scan with a resolution of 1 nm at a scan speed of 267 nm/min and a slit width of 2 nm. Liquid samples were analyzed in a quartz cuvette with a 10 mm path length, and solid samples were directly mounted to the sample holder.

**Steady-State Photoluminescence.** Steady-state PL spectroscopy was performed on a Fluorolog-3 spectrophotometer (Horiba Jobin Yvon). Solid-state emission spectra were recorded in both the front-face and edge emission configurations. The excitation and emission slits were adjusted so that the maximum PL intensity was within the range of linear response of the detector and were kept the same between samples if direct comparison between the emission intensity was required. PLQYs were measured using a Quanta-phi integrating sphere (Horiba Jobin Yvon) mounted on the Fluorolog-3 spectrophotometer. The values and errors reported are the mean and standard deviation of three repeating measurements. Emission and excitation spectra were corrected for the wavelength response of the system and the intensity of the lamp profile over the excitation range, respectively, using correction factors supplied by the manufacturer.

**FRET Calculations.** The Förster radius, $R_0$, defined as the donor−acceptor distance at which FRET is 50% efficient, was determined by the following equation[45]

$$R_0^6 = \frac{2.07}{128\pi^5 N_A}\frac{\kappa^2 Q_D}{n^4}\int F_D(\lambda)\epsilon_A(\lambda)\lambda^4\,d\lambda \quad (1)$$

where $N_A$ is Avogadro's number ($6.022 \times 10^{23}$), $\kappa^2$ is the dipole orientation factor (2/3 for isotropic orientation of the donor and acceptor), $Q_D$ is the quantum yield of the donor (0.45), $n$ is the refractive index of the medium (1.49), $F_D$ is the area-normalized emission spectrum of the donor, $\epsilon_A$ is the molar absorption coefficient spectrum of the acceptor (L $mol^{-1}$ $cm^{-1}$), and $\lambda$ is the photon wavelength (nm). The calculation was performed using the PhotochemCAD 3.0 software.[46,47]

**LSC Characterization.** The optical performance of LSCs was measured using a previously reported experimental setup.[10] In brief, the LSC was illuminated using a Class ABB solar simulator (Abet Technologies) equipped with an AM1.5G filter. A black absorptive mask with a circular aperture ($d$ = 3.5 cm) was placed on the top face of the LSC to clearly define the illumination area. The distance between the source of illumination and the LSC was calibrated according to the irradiance of 1 Sun (1000 ± 10 W $m^{-2}$) using a reference silicon solar cell (ReRa Technologies) coupled to a Keithley 2401 Sourcemeter. The emission from the edge of the LSC was collected by an INS125 integrating sphere (225−1400 nm, International Light Technologies) and directed to a spectroradiometer (SpectriLight ILT 950) through an optical cable. The spectrally resolved data in photocounts was collected from the spectroradiometer and calibrated into optical power ($\mu$W) using the calibration file ILT1007131U1NS123 through the SpectriLight III software. All


DOI: 10.1021/acsapm.9b00718
ACS Appl. Polym. Mater. 2019, 1, 3039−3047

measurements were performed on a black absorptive background. The parameters used to characterize the optical efficiencies of LSCs are the internal photon efficiency $\eta_{int}$ and external photon efficiency $\eta_{ext}$, defined by the following equations

$$\eta_{int} = \frac{N_{ph-out}}{N_{ph-abs}} = \frac{\sum_{i=1}^{4}\int_{250}^{1050} P_{i(out)}(\lambda)\frac{\lambda}{hc}\,d\lambda}{\int_{250}^{1050} P_{in}(\lambda)\frac{\lambda}{hc}(1-10^{-A(\lambda)})\,d\lambda} \quad (2)$$

$$\eta_{ext} = \frac{N_{ph-out}}{N_{ph-in}} = \frac{\sum_{i=1}^{4}\int_{250}^{1050} P_{i(out)}(\lambda)\frac{\lambda}{hc}\,d\lambda}{\int_{250}^{1050} P_{in}(\lambda)\frac{\lambda}{hc}\,d\lambda} \quad (3)$$

where $N_{ph-out}$ is the total number of edge-emitted photons summed over four edges ($i$ = 1−4) of the LSC, $N_{ph-abs}$ is the total number of photons absorbed by the LSC, and $N_{ph-in}$ is the total number of photons incident on the top surface of the LSC. $N_{ph-out}$ is obtained from the sum of the output power spectra, $P_{i(out)}(\lambda)$, measured for each edge of the LSC (in W nm$^{-1}$), where $\lambda$ is the wavelength of light (in nm). $P_{in}(\lambda)$ is the input power spectrum from the solar simulator incident on the top surface of the LSC (in W nm$^{-1}$), $h$ is Planck's constant (in J s), $c$ is the speed of light (in m s$^{-1}$), and $A(\lambda)$ is the absorption spectrum of the LSC. The integrations are performed over the full AM1.5G solar spectrum (250−1050 nm). The values and errors reported for $\eta_{int}$ and $\eta_{ext}$ are the mean and standard deviation of three repeat measurements, respectively.

## 3. RESULTS AND DISCUSSION

**Design Strategy.** Diureasil waveguides (denoted dU(600)) were synthesized via a two-step process, as illustrated in Figure 1. The first step involves coupling of the silane precursor ICPTES to a dibranched commercial polyetheramine, Jeffamine ED-600, to form the intermediate d-UPTES. The second step involves acid-catalyzed hydrolysis and condensation of the siliceous backbone, which after drying yields the final dU(600) waveguide as a free-standing monolith. The dU(600) structure consists of siliceous nanodomains (∼10 Å) covalently bonded to the Jeffamine chains via propylurea linkages.[48] To optimize the concentration of the donor p-O-TPE, as well as the concentration ratio between p-O-TPE and the acceptor PDI-Sil, we prepared three series of samples based on either p-O-TPE, PDI-Sil, or their mixtures incorporated into dU(600). In all samples, p-O-TPE is homogeneously mixed throughout the ureasil as a composite, whereas PDI-Sil is covalently grafted to the siliceous domains through the hydrolysis and co-condensation between the triethoxysilyl groups of PDI-Sil and d-UPTES during the sol−gel process.

As can be seen in Figure 2, p-O-TPE absorbs light in the UV/blue region (300−450 nm), which is complementary to the absorption range of PDI-Sil (400−600 nm). Therefore, by incorporating both lumophores in the same matrix, a larger portion of the solar spectrum will be absorbed, which is expected to enhance the absorption efficiency of the final LSC. Furthermore, Figure 2 demonstrates the excellent spectral overlap between the emission of p-O-TPE, which is centered at around 520 nm, and the absorption of PDI-Sil. The calculated critical Förster radius, $R_0$, defined as the average D−A separation required to achieve 50% FRET efficiency,[45] for the p-O-TPE-PDI-Sil pair (∼4.1 nm) is comparable to that of most previously reported D−A systems used in LSCs.[49,50] The ureasil waveguide itself can also harvest UV radiation and convert it into blue PL (Figure S1).[10,39,51] A previous study showed that FRET can also occur from the diureasil host to embedded lumophores with appropriate spectral overlap,

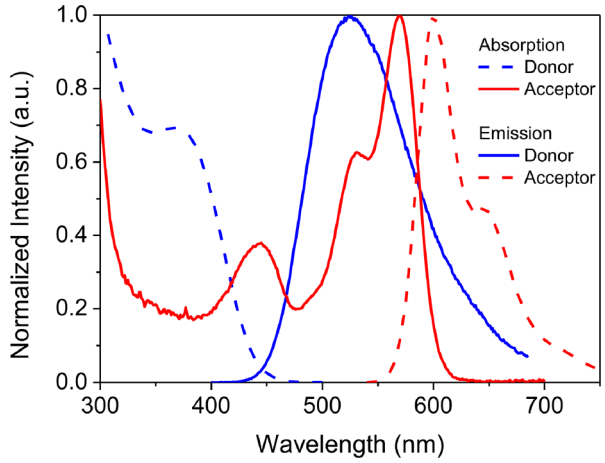


**Figure 2.** Normalized absorption (dashed blue) and emission (solid blue, $\lambda_{ex}$ = 380 nm) spectra of the donor (p-O-TPE) measured in 50 vol % EtOH/THF and normalized absorption (solid red) and emission (dashed red, $\lambda_{ex}$ = 520 nm) spectra of the acceptor (PDI-Sil) measured in THF. FRET is expected from p-O-TPE to PDI-Sil due to the large spectral overlap between the emission spectrum of p-O-TPE and absorption spectrum of PDI-Sil.

further extending the light-harvesting window of the final LSC.[10,39] We note that in Förster theory electronic coupling between the donor and acceptor is usually estimated by assuming the two species behave as point charges.[52] While this is a reasonable approximation when the molecular size is small compared to the intermolecular separation, experimental[53] and theoretical[54] studies suggest that this approximation may overestimate the energy transfer rate at short separation (<1 nm) for conjugated polymers, which exhibit extended transition dipole moment densities.

**Emission Properties of p-O-TPE as an AIEgen.** The aggregation of AIEgens can be induced either by introducing a bad solvent in solution or by forcing them to pack in a solid matrix.[32] In a good solvent (THF), p-O-TPE is only weakly emissive.[36] However, upon addition of a poor solvent (EtOH), a dramatic increase in the emission intensity up to 530% was observed (Figure S2). These results clearly demonstrate the AIE behavior of p-O-TPE in solution. To investigate whether the ureasil host could also induce this AIE behavior, p-O-TPE was doped into dU(600) at four different concentrations (0.001−0.05 wt % with respect to the dry monolith). Figure 3a shows photographs of the resultant p-O-TPE-dU(600) series under natural light. The green coloration of the samples becomes more intense as the concentration of p-O-TPE increases. The corresponding PL spectra are in good agreement with the solution data, with a broad emission band centered at ca. 513 nm (Figure 3b).

The PLQY of p-O-TPE increases dramatically from 2[36] to 44% (0.001 wt %) when moving from THF solution (used in the synthesis) to the ureasil matrix. We note that, as previously reported,[51,55] the blank ureasil is also weakly photoluminescent (PLQY = 4.1%, 0.00 wt % sample in Figure 3c). The PLQY of p-O-TPE increases further with increasing concentration, reaching a maximum of around 60% at 0.05 wt %. This is likely a result of increasing aggregation between p-O-TPE polymer chains in the ureasil matrix, which further rigidifies their molecular conformation. The formation of p-O-TPE aggregates in the ureasil is also apparent upon inspection of the samples under daylight conditions (Figure 3a), indicated by


DOI: 10.1021/acsapm.9b00718
ACS Appl. Polym. Mater. 2019, 1, 3039−3047

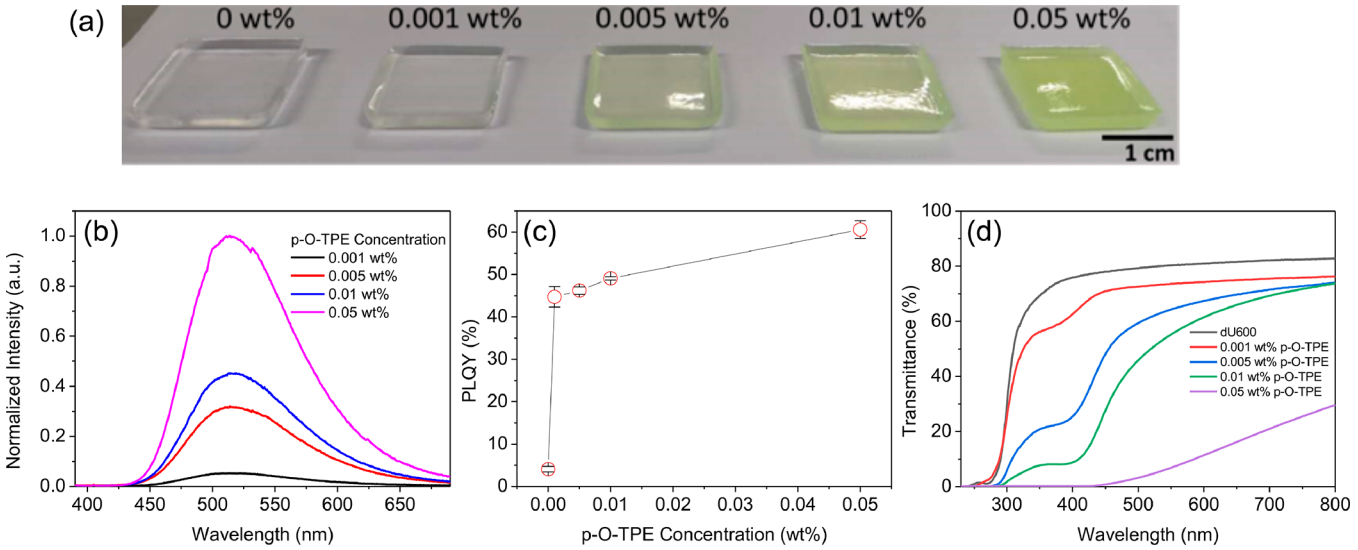


**Figure 3.** Optical properties of p-O-TPE-dU(600) ureasils. (a) Photographs of dU(600) doped with varying concentrations of p-O-TPE under daylight conditions. (b) Emission spectra ($\lambda_{ex}$ = 370 nm), (c) PLQY ($\lambda_{ex}$ = 400 nm), and (d) UV/vis transmittance spectra of p-O-TPE-dU(600) as a function of p-O-TPE concentration.

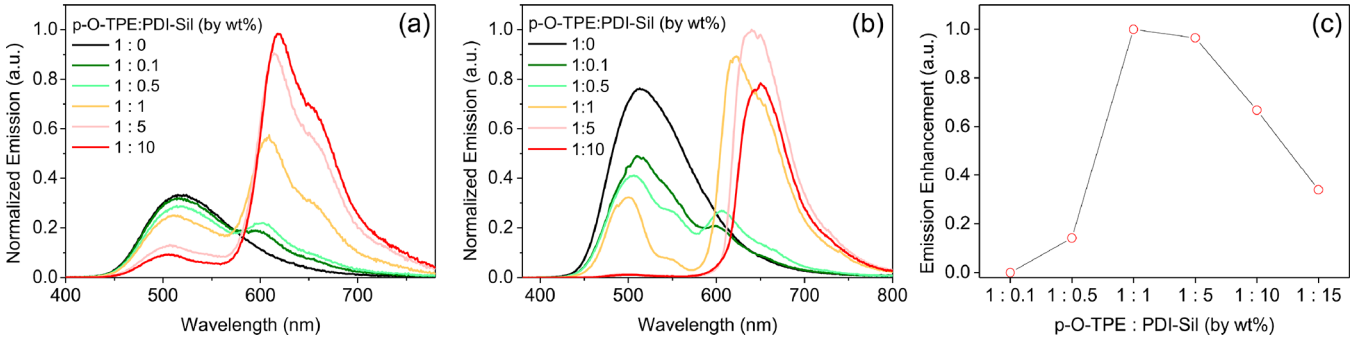


**Figure 4.** Optical properties of dU(600) ureasils (2 cm × 2 cm × 0.3 cm) doped with p-O-TPE and/or PDI-Sil. (a) Front-face and (b) edge emission spectra ($\lambda_{ex}$ = 370 nm) of p-O-TPE-PDI-Sil-dU(600) samples with various concentration ratios between p-O-TPE and PDI-Sil. (c) Enhancement in PDI-Sil emission for p-O-TPE-PDI-Sil-dU(600) as a function of the concentration ratio (by wt %) between p-O-TPE and PDI-Sil in arbitrary units.

the increasing opaqueness. These results demonstrate the emissive nature of the p-O-TPE aggregates formed in the ureasil matrix, as opposed to the typical ACQ behavior that is often observed for organic lumophores upon translation to the solid state.[29,32] The latter is often considered detrimental to the efficiency of the LSCs especially at the elevated concentrations required to maximize light harvesting.[3,11]

Despite the enhanced PLQY, scattering losses emerged as the concentration of p-O-TPE exceeded 0.005 wt %, caused by the increasing extent of aggregation. This is evident in the corresponding UV/vis transmittance spectra (Figure 3d), revealed by a significant loss of transmittance in the long-wavelength region where neither the diureasil nor p-O-TPE absorb. Such scattering losses will critically limit the optical efficiency of the LSC. Therefore, 0.005 wt % was chosen as the optimal concentration for the p-O-TPE donor as it represents the best compromise between a high PLQY without introducing scattering losses. We note that the ca. 10% reduction in the transmittance at 800 nm for the 0.001 wt % p-O-TPE sample compared to the blank is due to the presence of surface inhomogeneities introduced by the mold.

**Energy Transfer from p-O-TPE to PDI-Sil.** According to FRET theory, the energy transfer efficiency, *E*, strongly depends on the physical separation between the donor and acceptor molecules with an inverse sixth-power law.[45] Therefore, for a fixed concentration of p-O-TPE, the average physical separation between p-O-TPE and PDI-Sil is expected to be reduced by increasing the concentration of PDI-Sil, which will, in theory, lead to more efficient FRET. Due to the polymeric nature of p-O-TPE, it is not trivial to estimate the mean experimental separation of the donor and acceptor species at each concentration. To experimentally investigate the effect of varying PDI-Sil concentration on the FRET efficiency, a series of small LSC samples (2 cm × 2 cm × 0.3 cm) containing different p-O-TPE:PDI-Sil concentration ratios (by wt %) were fabricated. Figure 4a shows the emission spectra of the resulting p-O-TPE-PDI-Sil-dU(600) samples recorded in the front-face configuration upon excitation at 370 nm; at this excitation wavelength, light absorption is expected to occur primarily by p-O-TPE (Figure 2).

In the mixed samples, the PDI-Sil emission intensity increases steadily with concentration and is accompanied by a decrease in the p-O-TPE emission, which suggests the occurrence of FRET between the two lumophores (Figure 4a).[31,56,57] In addition, the characteristic excitation features of p-O-TPE are present in excitation spectra (Figure S3)


DOI: 10.1021/acsapm.9b00718
ACS Appl. Polym. Mater. 2019, 1, 3039−3047

selectively detected for PDI-Sil emission ($\lambda_{em}$ = 650 nm), which provides further evidence for the occurrence of FRET. However, PDI-Sil itself can also be moderately excited at 370 nm as the tail of its absorption band lies in this region (Figure 2). To determine the actual increase in acceptor emission due to FRET, the emission spectrum of PDI-Sil in the absence of p-O-TPE was investigated. A set of control samples doped with only PDI-Sil (PDI-Sil-dU(600)) at the same wt % were fabricated and their emission spectra were collected at $\lambda_{ex}$ = 370 nm (Figure S4). These spectra were then used to estimate the emission enhancement due to FRET at different D−A concentration ratios based on integrated photon counts (see the Supporting Information for a more detailed explanation of the emission enhancement calculation). For a p-O-TPE:PDI-Sil concentration ratio up to 1:1, an increase in the PDI-Sil concentration leads to significant enhancement in the PDI-Sil emission (Figure 4c). However, further increase in the concentration does not lead to additional enhancement in its intensity, despite the continued quenching of p-O-TPE emission (Figure 4a). It is plausible that, despite the improved spatial isolation expected through grafting,[39] PDI-Sil molecules begin to cluster in the siliceous nanodomains at concentrations higher than 0.005 wt % (the PDI-Sil concentration at which the donor−acceptor concentration ratio is 1:1). This may induce $\pi-\pi$ stacking interactions between the PDI-Sil molecules, which is also detectable in the normalized emission spectra of PDI-Sil-dU(600) (Figure S7), as indicated by the small red shift in the emission spectrum. As a result, the energy transferred from p-O-TPE to PDI-Sil may subsequently be lost through nonradiative relaxation, decreasing the efficiency.[10]

We note that trivial (nonradiative) energy transfer may also occur in these samples. However, if this were the dominant pathway, the increase in acceptor emission (in terms of the number of photons) would be expected to be much less than the corresponding reduction in donor emission due to the nonunity PLQY of the acceptor. Moreover, this trend would be exacerbated for successive radiative reabsorption events. In fact, at a concentration ratio of 1:1, the increase in PDI-Sil emission is greater than the reduction in p-O-TPE emission in the number of photons calculated by integrating the emission spectra (Figure S4). This suggests that radiative energy transfer is not the primary pathway. Moreover, it is conceivable that excitation energy that would have been lost due to nonradiative relaxation in p-O-TPE is instead transferred to PDI-Sil via FRET and re-emitted,[56,58] effectively increasing the PLQY of p-O-TPE from 46 to 67%.

In a working LSC device, the photons concentrated at the edge of the LSC travel through a much longer distance than those escaping from the surface, resulting in a significantly higher number of reabsorption events.[10] This is noticeable in the emission spectra detected at the edge of the samples (Figure 4b), where the quenching of p-O-TPE emission occurs much more rapidly due to additional radiative reabsorption events by PDI-Sil molecules along the long optical pathway to the edge, leading to the depletion of the p-O-TPE emission at concentration ratios higher than 1:1. In contrast, the relatively slower quenching of p-O-TPE emission detected at the front face of the slab (Figure 4a) is mostly due to the nonradiative FRET process from p-O-TPE to PDI-Sil. More importantly, as the p-O-TPE:PDI-Sil concentration ratio increases from 1:0.1 to 1:10, the emission from PDI-Sil undergoes significant spectral distortions and red shifts (Figure 4b) due to the increased reabsorption effects of the edge emission,[10] leading to greater losses of the PDI-Sil emission despite the increasing FRET efficiency. It was calculated that the LSC with a concentration ratio of 1:1 emits the highest number of photons at the edge (Figure S8) as a result of a balance between the increasing FRET efficiency and the growing reabsorption losses.

**Optical Efficiencies of the LSCs.** On the basis of the results above, p-O-TPE-PDI-Sil-dU(600) with a concentration ratio of 1:1 was considered the most promising candidate for a working LSC with a larger geometry because overall it offered the best compromise for FRET efficiency without introducing excessive scattering losses, nonradiative relaxation, and reabsorption at the edge of the slab. A set of larger doped LSCs (4.5 cm × 4.5 cm × 0.3 cm) based on the dU(600) waveguide, containing (1) both p-O-TPE and PDI-Sil (p-O-TPE-PDI-Sil-dU(600)), (2) only p-O-TPE (p-O-TPE-dU(600)), and (3) only PDI-Sil (PDI-Sil-dU(600)), were fabricated (Figure 5). All samples had the same concentrations

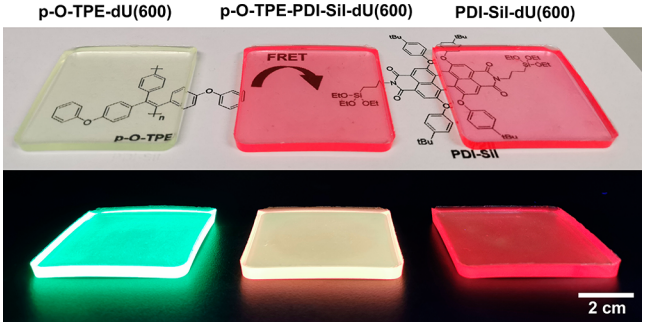


**Figure 5.** Photographs of p-O-TPE-dU(600) (left), p-O-TPE-PDI-Sil-dU(600) (middle), and PDI-Sil-dU(600) (right) under daylight (top) and UV irradiation (365 nm). Each sample contains 0.005 wt % of p-O-TPE and/or 0.005 wt % of PDI-Sil.

of p-O-TPE (0.005 wt %) and/or PDI-Sil (0.005 wt %). The UV/vis transmittance spectra are shown in Figure S9; we note that surface inhomogeneities from the mold were not present in these samples, leading to comparable transmittance at 800 nm for the blank and doped samples.

One of the key parameters to characterize the performance of LSCs is the internal photon efficiency ($\eta_{int}$),[56,59] defined as the ratio of the number of photons emitted from the edges to those absorbed by the LSC (eq 2), which quantifies the quality of the light-guiding process irrespective of the lumophore absorption range. Experimental $\eta_{int}$ values were determined by illuminating the top face of the planar LSCs using a solar simulator and measuring the edge output using a spectroradiometer-integrating sphere system (see the Experimental Section for further details). To achieve a high $\eta_{int}$, the lumophore needs to have a large Stokes shift to minimize reabsorption losses and a high PLQY to reduce nonradiative relaxation pathways.[60] In addition, scattering losses and internal emission trapping of the lumophore emission due to the waveguide material should be minimized.[60] The obtained $\eta_{int}$ values are summarized in Table 1.

As can be seen from Table 1, p-O-TPE-PDI-Sil-dU(600) demonstrates the highest $\eta_{int}$ of 20.0%, which is an improvement of 125 and 11% when compared to p-O-TPE-dU(600) and PDI-Sil-dU(600), respectively. While radiative energy transfer (i.e., from p-O-TPE to PDI-Sil) and self-reabsorption (for PDI-Sil) are certainly present, the dual-lumophore LSC


DOI: 10.1021/acsapm.9b00718
ACS Appl. Polym. Mater. 2019, 1, 3039−3047

Table 1. Internal ($\eta_{int}$) and External ($\eta_{ext}$) Photon Efficiencies of p-O-TPE-dU(600), p-O-TPE-PDI-Sil-dU(600), and PDI-Sil-dU(600), Determined over All Four Edges of the LSC with the Illumination of a Full AM1.5G Spectrum (250−1050 nm)[a]

| sample name | $\eta_{int}$ (%) | $\eta_{ext}$ (%) |
|---|---|---|
| p-O-TPE-dU(600) | 8.9 ± 0.4 | 1.9 ± 0.1 |
| PDI-Sil-dU(600) | 18.0 ± 0.1 | 4.6 ± 0.1 |
| p-O-TPE-PDI-Sil-dU(600) | 20.0 ± 0.1 | 5.5 ± 0.1 |

[a]The values and errors reported are the mean and standard deviation of three repeat measurements, respectively.

still outperforms the single-lumophore analogues. Comparison of $\eta_{int}$ values among the three LSC samples should be independent of both the lumophore absorption and waveguide. The higher $\eta_{int}$ for p-O-TPE-PDI-Sil-dU(600) relative to the $\eta_{int}$ of p-O-TPE-dU(600) sample can be understood in terms of reduced reabsorption losses due to the excitation energy cascade from the donor to acceptor, and the higher PLQY of PDI-Sil. The improvement in $\eta_{int}$ relative to the PDI-Sil-dU(600) sample is also attributable to these mechanisms. In addition, the dU(600) waveguide also absorbs light in the UV region (see Figure S1). This contribution will be negligible for the p-O-TPE-PDI-Sil-dU(600) and p-O-TPE-dU(600) samples as p-O-TPE has a much higher molar absorption coefficient in this region but could play a small role for PDI-Sil-dU(600). Previous studies have shown that dU(600) can undergo energy transfer to lumophores doped within its structure, including to LR305, which is a structural analogue of PDI-Sil.[10] However, it is very difficult to obtain evidence of this contribution in the p-O-TPE-PDI-Sil-dU(600) system due to strong overlap between the excitation spectra of dU(600) and p-O-TPE.

Another key figure of merit for evaluating the performance of an LSC is the external photon efficiency ($\eta_{ext}$),[12] defined as the ratio of the number of photons emitted from the edges of the LSC to that incident on top (eq 3). Unlike $\eta_{int}$, $\eta_{ext}$ is largely dependent on the absorption range of the lumophores. For a given $\eta_{int}$, the more incident photons the LSC absorbs, the higher the resulting $\eta_{ext}$ will be. As can be seen from Table 1, p-O-TPE-PDI-Sil-dU(600) again exhibits the highest $\eta_{ext}$ value of 5.5%, exceeding those of the individual p-O-TPE-dU(600) and PDI-Sil-dU(600) LSCs. The greater improvement in $\eta_{ext}$ compared to $\eta_{int}$ is believed to be due to the additional benefit from the extended absorption range provided by the two-lumophore system (Figure S10).

The $\eta_{int}$ value of 20.0% obtained for our p-O-TPE-PDI-Sil-dU(600) LSC is compared to recent literature values reported for LSCs calculated over the full AM1.5G spectrum in Table S1. The p-O-TPE-PDI-Sil-dU(600) LSC performs comparably to other FRET-based LSCs with a similar geometric gain (i.e., normalized for the LSC dimensions) but considerably underperforms compared to much larger LSCs incorporating QD lumophores. This trend highlights the limitations of molecular lumophore LSCs, which often have broad absorption and emission spectra, leading to reabsorption losses. Nonetheless, long-term questions of toxicity and resource availability still remain for QD LSCs. The use of aggregation-induced emitters as lumophores poses additional challenges due to the introduction of additional scattering defects. In the present system, a compromise was required to reduce scattering losses, leading to a less efficient FRET process. This is clearly not ideal, and a decrease in $\eta_{int}$ would be expected upon scale-up to larger devices. We are currently investigating the possibility of grafting the lumophore to the waveguide to induce AIE behavior, without the formation of large aggregates.

## 4. CONCLUSIONS

In summary, we have demonstrated a viable dual-lumophore system for LSCs based on FRET from p-O-TPE, an AIE conjugated polymer donor, to a red-emitting molecular acceptor (PDI-Sil), incorporated in a diureasil light guide. The diureasil host was shown to effectively induce AIE from p-O-TPE, although at higher concentrations the formation of large polymer aggregates led to scattering losses. A p-O-TPE concentration of 0.005 wt % was shown to be the best compromise between PLQY enhancement and minimized scattering losses. To reduce the extent of aggregation and prevent ACQ, the PDI-Sil acceptor molecules were covalently grafted to the siliceous domains of the diureasil. The concentration of PDI-Sil relative to p-O-TPE was optimized to give the highest FRET efficiency possible without introducing nonradiative decay losses and/or significant reabsorption of the emitted photons within the light guide. The resulting LSC based on the optimized p-O-TPE-PDI-Sil system showed improvement in its internal photon efficiency compared to the single-lumophore (p-O-TPE or PDI-Sil) LSCs, which was attributed to reduced loss of absorbed photons as a result of the FRET process. Enhancement in the external photon efficiency of the donor−acceptor LSC was also observed due to the extended solar-harvesting window provided by the complementary absorption spectra of the dual-lumophore system. The results also demonstrate the importance of lumophore−waveguide interactions in determining the final LSC efficiency. Here, the diureasil waveguide is used to promote aggregation and thus switch-on emission from the AIE donor, while simultaneously, covalent grafting of the acceptor reduces ACQ. This study therefore demonstrates that the bottom-up design of integrated lumophore−waveguide materials is a viable strategy to overcome the intrinsic optical losses of LSCs and to boost their solar-harvesting performance.

## ■ ASSOCIATED CONTENT

### Supporting Information

The Supporting Information is available free of charge on the ACS Publications website at DOI: 10.1021/acsapm.9b00718.

Photoluminescence properties of dU(600) light guides, AIE behavior of p-O-TPE in THF/EtOH solution, absorption spectra of large LSCs, and literature comparison of LSC efficiencies (PDF)

## ■ AUTHOR INFORMATION


### Corresponding Author

*E-mail: rce26@cam.ac.uk.

### ORCID

Sébastien Clément: 0000-0002-8473-8197

Rachel C. Evans: 0000-0003-2956-4857


### Notes

The authors declare no competing financial interest.



DOI: 10.1021/acsapm.9b00718
ACS Appl. Polym. Mater. 2019, 1, 3039−3047

## ■ ACKNOWLEDGMENTS

This project received funding from the European Research Council (ERC) under the European Union's Horizon 2020 research and innovation programme (Grant Agreement No. [818762]). This work was supported in part by an Isaac Newton Trust/University of Cambridge Early Career Support Scheme grant. S.C. thanks the CNRS and the Université de Montpellier for financial support.

## ■ REFERENCES

(1) Hermann, A. M. Luminescent Solar Concentrators-A Review. *Sol. Energy* **1982**, *29*, 323−329.
(2) Rowan, B. C.; Wilson, L. R.; Richards, B. S. Advanced Material Concepts for Luminescent Solar Concentrators. *IEEE J. Sel. Top. Quantum Electron.* **2008**, *14*, 1312−1322.
(3) Debije, M. G.; Verbunt, P. P. C. Thirty Years of Luminescent Solar Concentrator Research: Solar Energy for the Built Environment. *Adv. Energy Mater.* **2012**, *2*, 12−35.
(4) Meinardi, F.; Bruni, F.; Brovelli, S. Luminescent Solar Concentrators for Building-Integrated Photovoltaics. *Nat. Rev. Mater.* **2017**, *2*, 17072.
(5) Weber, W. H.; Lambe, J. Luminescent Greenhouse Collector for Solar Radiation. *Appl. Opt.* **1976**, *15*, 2299−2300.
(6) Reisfeld, R.; Neuman, S. Planar Solar Energy Converter and Concentrator Based on Uranyl-Doped Glass. *Nature* **1978**, *274*, 144−145.
(7) Reisfeld, R.; Kalisky, Y. Improved Planar Solar Converter Based on Uranyl Neodymium and Holmium Glasses. *Nature* **1980**, *283*, 281−282.
(8) Currie, M. J.; Mapel, J. K.; Heidel, T. D.; Goffri, S.; Baldo, M. A. High-Efficiency Organic Solar Concentrators for Photovoltaics. *Science* **2008**, *321*, 226−228.
(9) Mulder, C. L.; Reusswig, P. D.; Velázquez, A. M.; Kim, H.; Rotschild, C.; Baldo, M. A. Dye Alignment in Luminescent Solar Concentrators: I. Vertical Alignment for Improved Waveguide Coupling. *Opt. Express* **2010**, *18*, A79−A90.
(10) Kaniyoor, A.; Mckenna, B.; Comby, S.; Evans, R. C. Design and Response of High-Efficiency, Planar, Doped Luminescent Solar Concentrators Using Organic-Inorganic Di-Ureasil Waveguides. *Adv. Opt. Mater.* **2016**, *4*, 444−456.
(11) McKenna, B.; Evans, R. C. Towards Efficient Spectral Converters through Materials Design for Luminescent Solar Devices. *Adv. Mater.* **2017**, *29*, 1606491.
(12) Meinardi, F.; Colombo, A.; Velizhanin, K. A.; Simonutti, R.; Lorenzon, M.; Beverina, L.; Viswanatha, R.; Klimov, V. I.; Brovelli, S. Large-Area Luminescent Solar Concentrators Based on Stokes-Shift-Engineered Nanocrystals in a Mass-Polymerized PMMA Matrix. *Nat. Photonics* **2014**, *8*, 392−399.
(13) Li, H.; Wu, K.; Lim, J.; Song, H. J.; Klimov, V. I. Doctor-Blade Deposition of Quantum Dots onto Standard Window Glass for Low-Loss Large-Area Luminescent Solar Concentrators. *Nat. Energy* **2016**, *1*, 16157.
(14) Nolasco, M. M.; Vaz, P. M.; Freitas, V. T.; Lima, P. P.; André, P. S.; Ferreira, R. A. S.; Vaz, P. D.; Ribeiro-Claro, P.; Carlos, L. D. Engineering Highly Efficient Eu(Iii)-Based Tri-Ureasil Hybrids toward Luminescent Solar Concentrators. *J. Mater. Chem. A* **2013**, *1*, 7339−7350.
(15) Correia, S. F. H.; De Zea Bermudez, V.; Ribeiro, S. J. L.; André, P. S.; Ferreira, R. A. S.; Carlos, L. D. Luminescent Solar Concentrators: Challenges for Lanthanide-Based Organic-Inorganic Hybrid Materials. *J. Mater. Chem. A* **2014**, *2*, 5580−5596.
(16) Zhang, B.; Zhao, P.; Wilson, L. J.; Subbiah, J.; Yang, H.; Mulvaney, P.; Jones, D. J.; Ghiggino, K. P.; Wong, W. W. H. High-Performance Large-Area Luminescence Solar Concentrator Incorporating a Donor−Emitter Fluorophore System. *ACS Energy Lett.* **2019**, *4*, 1839−1844.
(17) Banal, J. L.; Ghiggino, K. P.; Wong, W. W. H. Efficient Light Harvesting of a Luminescent Solar Concentrator Using Excitation Energy Transfer from an Aggregation-Induced Emitter. *Phys. Chem. Chem. Phys.* **2014**, *16*, 25358−25363.
(18) Nketia-Yawson, B.; Lee, H. S.; Seo, D.; Yoon, Y.; Park, W. T.; Kwak, K.; Son, H. J.; Kim, B.; Noh, Y. Y. A Highly Planar Fluorinated Benzothiadiazole-Based Conjugated Polymer for High-Performance Organic Thin-Film Transistors. *Adv. Mater.* **2015**, *27*, 3045−3052.
(19) Liu, C.; Jang, J.; Xu, Y.; Kim, H. J.; Khim, D.; Park, W. T.; Noh, Y. Y.; Kim, J. J. Effect of Doping Concentration on Microstructure of Conjugated Polymers and Characteristics in N-Type Polymer Field-Effect Transistors. *Adv. Funct. Mater.* **2015**, *25*, 758−767.
(20) Ying, L.; Ho, C. L.; Wu, H.; Cao, Y.; Wong, W. Y. White Polymer Light-Emitting Devices for Solid-State Lighting: Materials, Devices, and Recent Progress. *Adv. Mater.* **2014**, *26*, 2459−2473.
(21) Zalar, P.; Henson, Z. B.; Welch, G. C.; Bazan, G. C.; Nguyen, T. Q. Color Tuning in Polymer Light-Emitting Diodes with Lewis Acids. *Angew. Chem., Int. Ed.* **2012**, *51*, 7495−7498.
(22) Duan, C.; Zhang, K.; Guan, X.; Zhong, C.; Xie, H.; Huang, F.; Chen, J.; Peng, J.; Cao, Y. Conjugated Zwitterionic Polyelectrolyte-Based Interface Modification Materials for High Performance Polymer Optoelectronic Devices. *Chem. Sci.* **2013**, *4*, 1298−1307.
(23) Wu, J. S.; Cheng, S. W.; Cheng, Y. J.; Hsu, C. S. Donor-Acceptor Conjugated Polymers Based on Multifused Ladder-Type Arenes for Organic Solar Cells. *Chem. Soc. Rev.* **2015**, *44*, 1113−1154.
(24) Huo, L.; Liu, T.; Sun, X.; Cai, Y.; Heeger, A. J.; Sun, Y. Single-Junction Organic Solar Cells Based on a Novel Wide-Bandgap Polymer with Efficiency of 9. 7%. *Adv. Mater.* **2015**, *27*, 2938−2944.
(25) Gutierrez, G. D.; Coropceanu, I.; Bawendi, M. G.; Swager, T. M. A Low Reabsorbing Luminescent Solar Concentrator Employing π-Conjugated Polymers. *Adv. Mater.* **2016**, *28*, 497−501.
(26) Yasarapudi, V. B.; Frazer, L.; Davis, N. J. L. K.; Booker, E. P.; Macmillan, A.; Gallaher, J. K.; Roberts, D.; Perrier, S.; Schmidt, T. W. Optimization of Energy Transfer in a Polymer Composite with Perylene Chromophores. *J. Mater. Chem. C* **2018**, *6*, 7333−7342.
(27) Meazzini, I.; Blayo, C.; Arlt, J.; Marques, A.-T.; Scherf, U.; Burrows, H. D.; Evans, R. C. Ureasil Organic−Inorganic Hybrids as Photoactive Waveguides for Conjugated Polyelectrolyte Luminescent Solar Concentrators. *Mater. Chem. Front.* **2017**, *1*, 2271−2282.
(28) Zhou, H.; Li, J.; Chua, M. H.; Yan, H.; Tang, B. Z.; Xu, J. Poly(Acrylate) with a Tetraphenylethene Pendant with Aggregation-Induced Emission (AIE) Characteristics: Highly Stable AIE-Active Polymer Nanoparticles for Effective Detection of Nitro Compounds. *Polym. Chem.* **2014**, *5*, 5628−5637.
(29) Banal, J. L.; White, J. M.; Ghiggino, K. P.; Wong, W. W. H. Concentrating Aggregation-Induced Fluorescence in Planar Waveguides: A Proof-of-Principle. *Sci. Rep.* **2015**, *4*, 4635.
(30) Banal, J. L.; White, J. M.; Ghiggino, K. P.; Wong, W. W. H. Concentrating Aggregation-Induced Fluorescence in Planar Waveguides: A Proof-of-Principle. *Sci. Rep.* **2014**, *4*, 4635.
(31) Zhang, B.; Banal, J. L.; Jones, D. J.; Tang, B. Z.; Ghiggino, K. P.; Wong, W. W. H. Aggregation-Induced Emission-Mediated Spectral Downconversion in Luminescent Solar Concentrators. *Mater. Chem. Front.* **2018**, *2*, 615−619.
(32) Hong, Y. Aggregation-Induced Emission—Fluorophores and Applications. *Methods Appl. Fluoresc.* **2016**, *4*, 022003.
(33) Mei, J.; Hong, Y.; Lam, J. W. Y.; Qin, A.; Tang, Y.; Tang, B. Z. Aggregation-Induced Emission: The Whole Is More Brilliant than the Parts. *Adv. Mater.* **2014**, *26*, 5429−5479.
(34) De Nisi, F.; Francischello, R.; Battisti, A.; Panniello, A.; Fanizza, E.; Striccoli, M.; Gu, X.; Leung, N. L. C.; Tang, B. Z.; Pucci, A. Red-Emitting AIEgen for Luminescent Solar Concentrators. *Mater. Chem. Front.* **2017**, *1*, 1406−1412.
(35) Ma, W.; Li, W.; Liu, R.; Cao, M.; Zhao, X.; Gong, X. Carbon dots and AIE molecules for highly efficiency tandem luminescent solar concentrators. *Chem. Commun.* **2019**, *55*, 7486−7489.
(36) Bayseç, S.; Preis, E.; Allard, S.; Scherf, U. Very High Solid State Photoluminescence Quantum Yields of Poly (Tetraphenylethylene) Derivatives. *Macromol. Rapid Commun.* **2016**, *37*, 1802−1806.
(37) Belton, C.; O'Brien, D. F.; Blau, W. J.; Cadby, A. J.; Lane, P. A.; Bradley, D. D. C.; Byrne, H. J.; Stockmann, R.; Hörhold, H. H.


DOI: 10.1021/acsapm.9b00718
*ACS Appl. Polym. Mater.* 2019, 1, 3039−3047

Excited-State Quenching of a Highly Luminescent Conjugated Polymer. *Appl. Phys. Lett.* **2001**, *78*, 1059−1061.
(38) Freitas, V. T.; Fu, L.; Cojocariu, A. M.; Cattoën, X.; Bartlett, J. R.; Le Parc, R.; Bantignies, J.-L.; Wong Chi Man, M.; André, P. S.; Ferreira, R. A. S.; Carlos, L. D. $Eu^{3+}$-Based Bridged Silsesquioxanes for Transparent Luminescent Solar Concentrators. *ACS Appl. Mater. Interfaces* **2015**, *7*, 8770−8778.
(39) Meazzini, I.; Willis-Fox, N.; Blayo, C.; Arlt, J.; Clément, S.; Evans, R. C. Targeted Design Leads to Tunable Photoluminescence from Perylene Dicarboxdiimide−Poly(Oxyalkylene)/Siloxane Hybrids for Luminescent Solar Concentrators. *J. Mater. Chem. C* **2016**, *4*, 4049−4059.
(40) Frias, A. R.; Pecoraro, E.; Correia, S. F. H.; Minas, L. M. G.; Bastos, A. R.; García-Revilla, S.; Balda, R.; Ribeiro, S. J. L.; André, P. S.; Carlos, L. D.; Ferreira, R. A. S. Sustainable Luminescent Solar Concentrators Based on Organic-Inorganic Hybrids Modified with Chlorophyll. *J. Mater. Chem. A* **2018**, *6*, 8712−8723.
(41) Bastos, A.; McKenna, B.; Lima, M.; André, P. S.; Carlos, L. D.; Evans, R. C.; Ferreira, R. A. S. Flexible Optical Amplifier for Visible-Light Communications Based on Organic-Inorganic Hybrids. *ACS Omega* **2018**, *3*, 13772−13781.
(42) Correia, S. F. H.; Lima, P. P.; André, P. S.; Ferreira, M. R. S.; Carlos, L. A. D. High-Efficiency Luminescent Solar Concentrators for Flexible Waveguiding Photovoltaics. *Sol. Energy Mater. Sol. Cells* **2015**, *138*, 51−57.
(43) Correia, S. F. H.; Frias, A. R.; Fu, L.; Rondão, R.; Pecoraro, E.; Ribeiro, S. J. L.; André, P. S.; Ferreira, R. A. S.; Carlos, L. D. Large-Area Tunable Visible-to-Near-Infrared Luminescent Solar Concentrators. *Adv. Sustain. Syst.* **2018**, *2*, 1800002.
(44) Buffa, M.; Carturan, S.; Debije, M. G.; Quaranta, A.; Maggioni, G. Dye-Doped Polysiloxane Rubbers for Luminescent Solar Concentrator Systems. *Sol. Energy Mater. Sol. Cells* **2012**, *103*, 114−118.
(45) Lakowicz, J. R. *Principles of Fluorescence Spectroscopy*; Springer, 2006.
(46) Du, H.; Fuh, R.-C. A.; Li, J.; Corkan, L. A.; Lindsey, J. S. PhotochemCADtt: A Computer-Aided Design and Research Tool in Photochemistry. *Photochem. Photobiol.* **1998**, *68*, 141−142.
(47) Dixon, J. M.; Taniguchi, M.; Lindsey, J. S. PhotochemCAD 2: A Refined Program with Accompanying Spectral Databases for Photochemical Calculations. *Photochem. Photobiol.* **2005**, *81*, 212−213.
(48) Meazzini, I.; Behrendt, J. M.; Turner, M. L.; Evans, R. C. Targeted $\beta$-Phase Formation in Poly(Fluorene)-Ureasil Grafted Organic-Inorganic Hybrids. *Macromolecules* **2017**, *50*, 4235−4243.
(49) Balaban, B.; Doshay, S.; Osborn, M.; Rodriguez, Y.; Carter, S. A. The Role of FRET in Solar Concentrator Efficiency and Color Tunability. *J. Lumin.* **2014**, *146*, 256−262.
(50) Bailey, S. T.; Lokey, G. E.; Hanes, M. S.; Shearer, J. D. M.; Mclafferty, J. B.; Beaumont, G. T.; Baseler, T. T.; Layhue, J. M.; Broussard, D. R.; Zhang, Y.; Wittmershaus, B. P. Optimized Excitation Energy Transfer in a Three-Dye Luminescent Solar Concentrator. *Sol. Energy Mater. Sol. Cells* **2007**, *91*, 67−75.
(51) Carlos, L. D.; Ferreira, R. A. S.; Pereira, R. N.; Assunção, M.; De Zea Bermudez, V. White-Light Emission of Amine-Functionalized Organic/Inorganic Hybrids: Emitting Centers and Recombination Mechanisms. *J. Phys. Chem. B* **2004**, *108*, 14924−14932.
(52) Brédas, J. L.; Beljonne, D.; Coropceanu, V.; Cornil, J. Charge-Transfer and Energy-Transfer Processes in $\pi$-Conjugated Oligomers and Polymers: A Molecular Picture. *Chem. Rev.* **2004**, *104*, 4971−5003.
(53) Pinto, S. M.; Burrows, H. D.; Pereira, M. M.; Fonseca, S. M.; Dias, F. B.; Mallavia, R.; Tapia, M. J. Singlet - Singlet Energy Transfer in Self-Assembled Systems of the Cationic Poly{9,9-bis[6-N,N,N-trimethylammonium)hexyl]fluorene-co-1,4-phenylene} with Oppositely Charged Porphyrins. *J. Phys. Chem. B* **2009**, *113*, 16093−16100.
(54) Wong, K. F.; Bagchi, B.; Rossky, P. J. Distance and Orientation Dependence of Excitation Transfer Rates in Conjugated Systems: Beyond the Förster Theory. *J. Phys. Chem. A* **2004**, *108*, 5752−5763.
(55) Willis-Fox, N.; Marques, A. T.; Arlt, J.; Scherf, U.; Carlos, L. D.; Burrows, H. D.; Evans, R. C. Synergistic Photoluminescence Enhancement in Conjugated Polymer-Di-Ureasil Organic-Inorganic Composites. *Chem. Sci.* **2015**, *6*, 7227−7237.
(56) Tummeltshammer, C.; Portnoi, M.; Mitchell, S. A.; Lee, A. T.; Kenyon, A. J.; Tabor, A. B.; Papakonstantinou, I. On the Ability of Förster Resonance Energy Transfer to Enhance Luminescent Solar Concentrator Efficiency. *Nano Energy* **2017**, *32*, 263−270.
(57) Banal, J. L.; Soleimaninejad, H.; Jradi, F. M.; Liu, M.; White, J. M.; Blakers, A. W.; Cooper, M. W.; Jones, D. J.; Ghiggino, K. P.; Marder, S. R.; Smith, T. A.; Wong, W. W. H. Energy Migration in Organic Solar Concentrators with a Molecularly Insulated Perylene Diimide. *J. Phys. Chem. C* **2016**, *120*, 12952−12958.
(58) Pandya, R.; Macqueen, R. W.; Rao, A.; Davis, N. J. L. K. Simple and Robust Panchromatic Light Harvesting Antenna Composites via FRET Engineering in Solid State Host Matrices. *J. Phys. Chem. C* **2018**, *122*, 22330−22338.
(59) Sol, J. A. H. P.; Timmermans, G. H.; van Breugel, A. J.; Schenning, A. P. H. J.; Debije, M. G. Multistate Luminescent Solar Concentrator "Smart" Windows. *Adv. Energy Mater.* **2018**, *8*, 1702922.
(60) Wei, M.; de Arquer, F. P. G.; Walters, G.; Yang, Z.; Quan, L. N.; Kim, Y.; Sabatini, R.; Quintero-Bermudez, R.; Gao, L.; Fan, J. Z.; Fan, F.; Gold-parker, A.; Toney, M. F.; Sargent, E. H. Ultrafast Narrowband Exciton Routing within Layered Perovskite Nanoplatelets Enables Low-Loss Luminescent Solar Concentrators. *Nat. Energy* **2019**, *4*, 197−205.


DOI: 10.1021/acsapm.9b00718
*ACS Appl. Polym. Mater.* 2019, 1, 3039−3047